

Quantum oscillations and linear magnetoresistance in ultraclean CaVO₃ thin films

Mahni Müller¹, Maria Espinosa¹, Olivio Chiatti¹, Tatiana Kuznetsova², Roman Engel-Herbert^{2,3} and Saskia F. Fischer^{1,4}

¹ Novel Materials Group, Institute of Physics, Humboldt-Universität zu Berlin, Newtonstr. 15, 12489 Berlin, Germany

² Department of Materials Science and Engineering, The Pennsylvania State University, University Park, PA 16802 USA

³ Paul Drude Institute for Solid State Electronics, Hausvogteiplatz 5-7, 10117 Berlin, Germany.

⁴ Center of the Sciences of Materials Berlin, Humboldt-Universität zu Berlin, Zum Großen Windkanal 2, 12489 Berlin, Germany

Advances in epitaxy of transition metal oxides with perovskite structure allow novel insights into transport mechanisms of strongly correlated electron systems, which are of interest for future transparent electronics. In this study, we investigate magnetotransport properties of thin epitaxial CaVO₃ films, grown coherently strained on LaAlO₃, and demonstrate for the ultraclean limit quantum oscillations. Fermi liquid behavior is detected in the temperature-dependent resistivity $\rho(T) \sim T^2$ up to 20 K, with effective mean free paths exceeding up to 20 times the film thickness (38 nm). Shubnikov-de Haas oscillations and a non-linear Hall resistance reveal two electron-like (1 and 2) and one hole-like (h) carriers, reflecting the three-fold Fermi surface of orthorhombic CaVO₃, with effective charge carrier densities and mobilities at 4.2 K of: (1) $n_1 \approx 9.3 \cdot 10^{21} \text{ cm}^{-3}$ with low mobility $\mu_1 \approx 926 \text{ cm}^2 \text{ V}^{-1} \text{ s}^{-1}$, (2) $n_2 \approx 7.2 \cdot 10^{19} \text{ cm}^{-3}$ with high mobility $\mu_2 \approx 6600 \text{ cm}^2 \text{ V}^{-1} \text{ s}^{-1}$, and (h) $n_h \approx 2.2 \cdot 10^{18} \text{ cm}^{-3}$ with $\mu_h \approx 1500 \text{ cm}^2 \text{ V}^{-1} \text{ s}^{-1}$. A non-saturating linear magnetoresistance dominates at low temperatures, exceeding the value for single crystals by 30%. Our findings

on epitaxial films demonstrate the delicate interplay of multiple carriers with correlations stemming from a non-spherical nested Fermi surface of a perovskite structure with orthorhombic distortion.

I. INTRODUCTION

Transparent conductors are in high demand for optoelectronics and require both high transparency and high conductivity¹⁻⁶. Typical doped wide band-gap semiconductors (e. g. ITO, ZnO) face limitations due to the increased charge carrier scattering⁷ and are aimed to be replaced by more abundant materials⁸. Correlated metals offer high electrical conductivity and optical transparency, due to increased electron-electron correlations and a high effective mass⁹. CaVO_3 and SrVO_3 are correlated metals with an ABO_3 perovskite-type crystal structure and a $3d^1$ electron configuration, and are often described as Fermi liquids^{9,10}. While the crystal structure of CaVO_3 is orthorhombic, SrVO_3 is cubic. Despite its smaller lattice parameter and thus larger orbital overlap, the orthorhombic distortion is expected to decrease the electronic bandwidth, which increases electron localization¹¹⁻¹³ and hence the effective mass¹⁴, placing CaVO_3 closer to the Mott transition^{2,11}. Improvements of oxide thin film growth allows synthesizing epitaxial films of highest quality with low defect concentration¹⁵. Recent reports¹⁶ on the intrinsic transport properties of SrVO_3 in the ultraclean limit reveal deviations from the normal Landau-Fermi liquid description, by detection of an anomalously high Hall coefficient and a scattering time anisotropy at 4 K. Studies using photoemission spectra (PES) and local density approximation and dynamical mean-field theory (LDA + DMFT), have revealed that the electronic structure and Fermi surface geometry of CaVO_3 and SrVO_3 are similar^{19,20}. Calculations reveal a three-fold Fermi surface^{9,17,18}. To date, several open issues persist: for thin films no quantum oscillations^{2,27} have been reported; the differences between CaVO_3 and

SrVO₃ in correlation effects and the origin of a non-saturating linear magnetoresistance in both call for further investigations.

In this study, we demonstrate that quantum oscillations, which are intrinsic to CaVO₃ single crystals^{2,27}, are also observed in high-quality epitaxial thin films and, further, that an enhanced non-saturating linear magnetoresistance appears at low temperatures. Systematically, we investigate the temperature-dependent magnetotransport of a series of CaVO₃ thin films with increasing crystal quality, quantified by the residual resistivity ratio RRR (from 2 to 90). From the temperature-dependent resistance the scattering mechanisms are analyzed via the exponent α of a power-law behavior and the Fermi liquid behavior is discussed for $\alpha = 2$. An approximative two carrier fit to the magnetoresistance and Hall resistance is performed at lower magnetic fields up to 6 T. The full three Fermi surface theory is approached by the identification of a third carrier channel at higher fields up to 12 T. We discuss the outcomes with previous results published for CaVO₃ single crystals^{1,2,27} and comparable SrVO₃ thin epitaxial films¹⁶, showing that the transport characteristics from CaVO₃ epitaxial films of highest quality differ from both. The results indicate how transport properties can be tailored by size control of coherently applied small strain and/or increased surface scattering in epitaxial thin films of these correlated metals.

II. RESULTS

The structural properties of the films under various growth conditions were investigated in detail in Ref. 21. Growth control and surface reconstruction was monitored by RHEED patterns for determination of film surface crystallinity and smoothness. Atomically flat films with terrace-like morphology and rms roughness values as low as 1.32 Å were found for films grown at VTIP pressures between 75 and 83 mTorr. This is the growth window for the epitaxial films of the highest quality, as confirmed by transport measurements in Ref. 21 and this work.

Here, we present the temperature-dependent resistivity of CaVO_3 films synthesized under these different growth conditions in Fig. 1(a). The residual resistivity ratio $RRR = \frac{\rho(300 \text{ K})}{\rho(4.2 \text{ K})}$ was determined, which is a measure for the crystalline quality in macroscopic samples and serves as a lower limit for size-constrained mesoscopic transport in thin film layers²⁹. Considering the film thickness of 38 nm, the maximum value of $RRR = 98$ for CaVO_3 on LaAlO_3 is comparable to that of bulk single crystals^{1,2} ($RRR_{\text{max}} \approx 200$) and thicker films^{26,28} of CaVO_3 on SrTiO_3 ($RRR_{\text{max}} \approx 1200$). In the ultraclean limit, we determine a minimal residual resistivity of $\rho(T = 4.2 \text{ K}) \approx 3.6 \cdot 10^{-7} \Omega \text{ cm}$ ($RRR = 98$).

An approximate expression of the temperature-dependent resistivity $\rho(T) = \rho_0 + A \cdot T^\alpha$ is used in order to analyze the scattering mechanisms, with the exponent $\alpha(T) = \frac{\partial \log(\rho(T) - \rho_0)}{\partial \log T}$, as shown in Fig. 1(b). At room temperature $\alpha \approx 2$ is found for all films. With decreasing temperature, α increases and reaches a maximum of $\alpha = 2.8$ to 3.2 around 30 K and 60 K for films in the ultraclean and disordered limit, respectively. Below 20 K, the films with $RRR > 90$ show an $\alpha \approx 2$ dependence, whereas the films with $RRR \leq 10$ show a varying $\alpha < 3$. Below $T \approx 1 \text{ K}$ all films reach a constant residual resistivity ρ_0 (see also Supplementary Material S1). As depicted in Fig. 1(b), α for a SrVO_3 thin film in the ultraclean regime¹⁶ agrees well with the temperature behavior for equivalent CaVO_3 films ($RRR > 68$).

A change in the exponent α indicates a crossover of the dominant scattering mechanism, from which we identify three temperature regimes: (i) At low temperatures ($T < 20 \text{ K}$) electron-electron scattering dominates and results in a T^2 -dependence³³. This has been observed for CaVO_3 single crystals^{1,2} and thin films^{24,26,28}, and for epitaxial SrVO_3 thin films^{16,34}. However, for lower crystalline quality ($RRR = 2$) our results indicate that the low-temperature resistivity is dominated by impurity scattering. (ii) At intermediate temperatures the temperature dependence of α is similar to that of transition metals with to s - d scattering, often associated

with the Bloch-Wilson limit⁴⁰⁻⁴² ($\alpha = 3$). For instance, high-purity vanadium samples⁴¹ exhibit a peak in $\alpha \approx 3$ at 40 K (see Supplementary Material S2). In CaVO_3 , the density of states of the V $3d$ and O $2p$ orbitals near the Fermi energy^{19,31} suggests that a similar physical mechanism could result in a T^3 -dependence. (iii) At higher temperatures $\alpha \approx 2$ is observed above 200 K (Fig. 1(b)) and for SrVO_3 thin epitaxial films^{34,38} above 100 K. Theoretically, an increased Hubbard-Coulomb interaction increases the effective electron-phonon coupling^{36,37}, increasing the electron-phonon scattering and the effective mass³⁴ $m_{\text{e-ph}}^*$. Further, dynamical mean field theory calculations³⁸ for SrVO_3 attribute $\alpha \approx 2$ at higher temperatures to electron-phonon scattering with an increased contribution from optical phonons³⁸. Other proposals³⁴ discuss $\alpha \approx 2$ at higher temperatures in terms of electron-phonon scattering on cylindrical Fermi surfaces³⁹ or of polaronic transport due to an enhanced electron-phonon coupling³⁴. We propose that our observations for CaVO_3 epitaxial thin films share common physical origins with those in SrVO_3 , given the similarities in band structure, Fermi surfaces^{19,20} and Debye temperature θ_D , despite discrepancies in absolute values reported in the literature^{3,31} for θ_D .

The temperature dependence of transport material parameters is depicted in Fig. 1(c) and Fig. 1(d). For very low magnetic fields ($|B| \leq 700$ mT) the Hall resistance R_{xy} was measured and the Hall coefficient was determined as $R_H = \frac{\partial R_{xy}}{\partial B}$. A first characterization is obtained by analyzing these low-field magnetotransport data within a one-band model approximation: the *effective* carrier density n_{eff} is the inverse Hall coefficient, $n_{\text{eff}} = (-eR_H)^{-1}$, and the *effective* mobility μ_{eff} is given by $\mu_{\text{eff}} = (e n_{\text{eff}} \rho)^{-1}$, where ρ is the resistivity in zero magnetic field. When evaluated in this manner, below 100 K the CaVO_3 films show a strong increase in $\mu_{\text{eff}}(T)$ with decreasing temperature, consistent with a decrease in electron-phonon scattering. For the highest RRR the largest increase in μ_{eff} is observed. While the effective carrier density n_{eff} at room temperature is nearly the same for all films, its significant temperature-dependent decrease is strongly RRR dependent. For highest RRR the largest decrease in n_{eff} of 33 % from

room temperature to 4.2 K is observed. From the values of $\mu_{\text{eff}}(T)$ and $n_{\text{eff}}(T)$ a temperature-dependent *effective* electronic mean free path (MFP) $l_e = \frac{\hbar}{e} \mu_{\text{eff}} \cdot (3\pi^2 n_{\text{eff}})^{\frac{1}{3}}$ can be derived, as shown in Fig. 1(d). For high RRR a value of up to $l_e \approx 860$ nm at 4.2 K is determined, exceeding the film thickness of $d = 38$ nm by an order of magnitude. Therefore, elastic scattering at the surfaces and interfaces of the films plays an important role for $RRR > 26$, as compared to CaVO_3 single crystals. This leads to anisotropic scattering by extrinsic size effects. However, intrinsic anisotropies due to the band structure require more than a one-band model, which does not account for the three-fold Fermi surface in CaVO_3 and its anisotropies. Intrinsically, scattering times for different bands may vary significantly over the Fermi surface, as has been discussed for SrVO_3 ¹⁶.

Magnetotransport at higher fields up to 6 T provides more detailed information for a multi-band model. The longitudinal magnetoresistance $MR = \frac{R_{xx}(B)}{R_{xx}(B=0)} - 1$ is shown in Fig. 2, for higher epitaxial quality ($RRR = 60$) in Fig. 2(a) and for lower quality ($RRR = 2$) in Fig. 2(e). A striking change in the MR for $RRR = 60$ is observed in magnitude when cooling from 80 K down to 4 K (with a maximum of 4 % at 80 K and of 44% at 4 K), which can be related to the increase of μ_{eff} with decreasing temperature. Accordingly, the field dependence of the magnetoresistance displays increasingly linear behavior below $T < 20$ K. The data were fitted with $MR = a_{MR}|B| + b_{MR} \cdot B^2 + c_{MR} \cdot |B^3|$ with linear, quadratic and cubic MR coefficients a_{MR} , b_{MR} and c_{MR} , shown in Fig. 2(b)-(d), respectively. The cubic term improves the fit and may arise from effects at higher fields, as discussed below. The linear coefficient a_{MR} is negligible at higher temperatures above 60 K and increases continuously with decreasing temperature. In contrast, the quadratic coefficient b_{MR} has a maximum around $T \approx 30 - 40$ K, which coincides with the maximum exponent α of the temperature-dependent resistivity. At

temperatures below 40 K the linear component dominates and we find $a_{MR} \cdot |B| \gg b_{MR} \cdot B^2 \gg |c_{MR} \cdot B^3|$.

The corresponding MR data for the lowest epitaxial quality ($RRR = 2$) is shown in Fig. 2(e). In the field dependence, the MR does not display a dominant linear behavior below $T < 20$ K. The fitting coefficients are shown in Fig. 2(f)-(h) and reveal a qualitatively similar temperature dependence as for the films of higher epitaxial quality, but with magnitudes of a factor 100 smaller for a_{MR} and a factor 10 smaller for b_{MR} .

These features of the field dependence can be clearly observed when MR is plotted as a function of $\mu_{\text{eff}}B$, as shown in Fig. 3(a) and b. For $RRR = 60$ (Fig. 3(a)) three temperature regimes become obvious: (I) the low-temperature regime with a dominant linear MR below 20 K; (II) the intermediate temperature regime, displaying a significant linear contribution to MR (from 20 K to 60 K); and (III) the high-temperature regime, with a dominant quadratic term above 60 K. Instead for the disordered limit $RRR = 2$ (Fig. 3(b)), the field dependences of all temperatures resemble regime (III) of Fig. 2(a) ($\beta \approx 1.58$). This indicates that intrinsic multi-band contributions become evident for higher epitaxial quality at lower temperatures, and interestingly the temperature regimes below 20 K (i) from the zero-field resistivity and (I) from the magnetoresistance coincide.

Further, a double-logarithmic plot of MR as a function of $\mu_{\text{eff}}B$, as depicted in Fig. 3(c), clearly shows the power-law behavior $MR \sim B^\beta$ and a crossover of the exponents from the temperature regime (I): $\beta \approx 1$ to (III): $\beta \approx 1.65$. This is detailed in Fig. 3(d) for both $RRR = 60$ and $RRR = 2$, showing further the striking difference of a factor 100 of the MR at low temperatures between high and low epitaxial quality films.

The temperature-dependent transversal Hall resistance R_{xy} up to 6 T for the higher quality epitaxial film ($RRR = 60$) shows non-linearities below 100 K, indicating multi-carrier transport. In Fig. 4(a), these are displayed by the numerical derivative of the Hall resistance

$\frac{\partial R_{xy}}{\partial B}$. It is nearly constant from room temperature down to 100 K. In the range $100 \text{ K} > T > 60 \text{ K}$, a small maximum can be seen at $B = 0$, consistent with a small hole contribution. Below 60 K a minimum appears at zero magnetic field, which increases in magnitude down to 4.2 K. This is indicative of the appearance of a second electron channel. In contrast, the film with $RRR = 2$ shows a constant derivative at all temperatures (see Supplementary Material S3), which indicates that defect-induced scattering limits the mobilities and mask multi-carrier transport phenomena.

Because the Fermi surface in CaVO_3 is triply degenerate, we attribute these changes in the Hall slope to carriers from different bands³¹. From Fig. 4(a) the contribution of a hole channel is expected to be negligible, therefore we apply first a two-band model with $R_{xy}(B) = -\frac{B}{e} \cdot$

$\frac{(n_1\mu_1^2+n_2\mu_2^2)+\mu_1^2\mu_2^2(n_1+n_2)B^2}{(n_1\mu_1+n_2\mu_2)^2+\mu_1^2\mu_2^2(n_1+n_2)^2B^2}$ (see Supplementary Material S4 and S5). From the fits we obtain

electron mobilities and densities as shown in Fig. 4(b)-(c). The results indicate one channel with a large electron density n_1 and low mobility μ_1 , and a second channel with a smaller electron density n_2 and higher mobility μ_2 . At $T = 4.2 \text{ K}$ we obtain: for channel 1, $n_1 \approx 9.3 \cdot 10^{21} \text{ cm}^{-3}$ and $\mu_1 \approx 926 \text{ cm}^2 \text{ V}^{-1} \text{ s}^{-1}$; for channel 2, $n_2 \approx 7.2 \cdot 10^{19} \text{ cm}^{-3}$ and $\mu_2 \approx 6600 \text{ cm}^2 \text{ V}^{-1} \text{ s}^{-1}$. The temperature dependence of n_1 is similar to the effective carrier density n_{eff} , indicating that channel 1 is the dominant transport contribution. The electron density of channel 2 is $n_2 \approx 1.5 \cdot 10^{18} \text{ cm}^{-3}$ for temperatures above $T \approx 50 \text{ K}$ and increases with decreasing temperature. The linear contribution to the magnetoresistance a_{MR} and the electron density of channel 2 have similar temperature dependences, therefore indicating that channel 2 is the dominant contribution to the linear magnetoresistance and responsible for the minimum at $B \approx 0$ in the Hall slope. Both channels show similar temperature dependence of the mobility. Therefore, the two-band model appears sufficient to describe the non-linear Hall effect at intermediate magnetic fields in CaVO_3 high-quality epitaxial layers. While non-

linearities in the Hall resistance have been previously found in SrVO₃ epitaxial layers in the ultraclean limit, those results differ because a pronounced hole contribution was observed down to low temperatures [16].

In order to test whether the magnetoresistance saturates and quantum oscillations for $\mu_{\text{eff}}B \gg 1$ can be observed, high-field transport measurements up to 12 T were performed. In Fig. 5(a) and (b) the magnetoresistance and Hall resistance data, respectively, are shown for the CaVO₃ thin film with $RRR = 64$ in the temperature range from 100 K to 50 mK. Strikingly, the magnetoresistance does not saturate up to 12 T. A non-saturating linear magnetoresistance (LMR) has been reported for single crystals¹, where magnetoresistance and magnetization anisotropies have been accounted for by an open orbit along the (110) direction, leading to an absence of saturation of the positive magnetoresistance.

In Fig. 5(c) the temperature dependence of the numerical derivative of the magnetoresistance reveals several features: at 100 K the quadratic field dependence is dominant, while at the lowest temperature of 50 mK the low-field regime (< 0.2 T) is predominantly quadratic and therefore distinct from the high-field regime (> 0.2 T) of a dominant linear component with a minor quadratic contribution. Below 45 K the MR slope shows the onset of quantum oscillations at fields above 7 T. In Fig. 5(d), the temperature dependence of the numerical derivative of the Hall resistance confirms this, such as the maximum at $B = 0$ for $T > 60$ K, the minimum for $T < 60$ K and the quantum oscillations above 7 T and below 45 K. Two-band fits yield results consistent with those in Fig. 4.

The quantum oscillations in the MR and Hall slopes at 50 mK are field-symmetric, as depicted in Fig. 6(a) (as a function of the absolute value of the magnetic field $|B|$). The Hall slope oscillation is periodic in $\frac{1}{B}$, as shown in Fig. 6(b), with a period of $\Delta\left(\frac{1}{B}\right) = \frac{0,019}{\text{T}}$. This is consistent with Shubnikov-de-Haas (SdH) oscillations of a frequency $B_{\text{SdH}} \approx 52$ T. From

$\Delta\left(\frac{1}{B}\right) = \frac{2\pi e}{\hbar} S_F^{-1}$ we determine a carrier density³², assuming that $S_F = \pi k_F^2 = \pi(3\pi^2 n_{\text{SdH}})^{\frac{2}{3}}$ is the relevant cross-section of the Fermi surface. The corresponding carrier density is $n_{\text{SdH}} \approx 2.2 \cdot 10^{18} \text{ cm}^{-3}$, much smaller than the electron densities from the two-band fits. From the results of Fig. 4 and 5, a hole channel with smaller carrier density than both electron channels is expected. Therefore, the hole channel may account for the observed quantum oscillations. The corresponding mobility can be estimated from the lowest magnetic field B_{min} , where quantum oscillations are observed: $\mu_{\text{h}} = (B_{\text{min}})^{-1} \approx 1500 \text{ cm}^2/\text{Vs}$. These results confirm the excellent quality of the epitaxial CaVO_3 layers in the ultraclean limit. SdH oscillations are known from CaVO_{3-y} single crystals² ($RRR = 20, B_{\text{SdH}} = 300 \text{ T}$), however, for ultraclean SrVO_3 epitaxial layers ($RRR = 195$) no SdH oscillations were reported¹⁶ up to 18 T.

III. DISCUSSION

In the following we discuss our experimental results in the *ultraclean* limit in the context of previous reports. In general, the temperature dependence of the resistivity ρ of our epitaxial 38 nm thin films of CaVO_3 on LaAlO_3 resembles that of bulk CaVO_3 single crystals^{1,2} and is similar to that of ultraclean SrVO_3 epitaxial layers¹⁶. We identify three temperature regimes with power law behavior (exponent α) of the correlated metal: (i) Fermi liquid behavior ($\alpha \approx 2$) at low temperatures dominated by electron-electron scattering¹⁶, (ii) an intermediate temperature regime ($2.8 < \alpha < 3.2$) as a cross-over to a (iii) high temperature regime ($\alpha \approx 2$), where charge carrier scattering is distinguished from normal metal behavior by effects of correlation, the three-fold Fermi surface and intrinsic anisotropic scattering in k -space¹⁶.

A first important outcome is that the high-quality thin epitaxial films of CaVO_3 on LaAlO_3 compare well with the best single crystals^{1,2}. However, the range of lowest temperatures in the regime (i) which shows a constant residual resistivity is reduced by almost a factor 10 for the epitaxial films (4 K) as compared to that of single crystals^{1,2} (30 K). This indicates that finite

size effects may play a role in enhancing electron-phonon scattering as the effective mean free path exceeds the film thickness (Fig. 1(d)).

Similarly, the magnetoresistance results compare well with those reported before^{1,2,16}. A positive magnetoresistance is indicative for stoichiometric CaVO_3 with standard magnetic-field induced carrier localization. In thin films, finite size effects and substrate-induced tensile strain (0.47%) may be the origin for an *enhanced* magnetoresistance (32% at 5 T, 4 K) as compared to single crystals¹ (2% at 5 T, 2 K).

From the power law behavior (exponent β) of the field dependence of the magnetoresistance at different temperatures (Fig. 3) we identify three temperature regimes: (I) ($\beta \approx 1$) at low temperatures up to 20 K, where a non-saturating LMR dominates, corresponding to the temperature regime (i) of the Fermi liquid behavior, and the resistivity is dominated by the second electron channel identified by the multi-band fit (Fig. 4); (II) ($\beta \approx 1.33$) in an intermediate temperature regime (20 – 60 K) and (III) ($\beta \approx 1.65$) in the high-temperature regime, with a dominant B^2 -term above 60 K. This kind of analysis is not yet widespread for CaVO_3 ; however, it reveals clearly a strongly enhanced *MR* at low temperatures distinguishing the ultraclean and the disordered limit. In the ultraclean limit decreased defects densities may enhance transport in open orbits on the Fermi surface. Additionally, in epitaxial films the electronic bandwidth and local site environment may be sensitive to charge redistribution, confinement and epitaxial strain inducing changes in the V-O bond lengths and V-O overlap/hybridization¹¹.

The ultimate proof that we have approached the ultraclean limit, is given by the Shubnikov-de Haas oscillations with a frequency of 52 T (Fig. 6(b)) at high magnetic fields, which we attribute to the hole channel. The occurrence of quantum oscillations confirms a crystalline quality equivalent to single crystals^{2,27}. For CaVO_3 single crystals²⁷ a de-Haas-van-Alphen frequency of 5000 T is reported; however, this frequency cannot be observed within the

magnetic field range up to 12 T in this study. Further, off-stoichiometric CaVO_{3-y} single crystals² show a SdH oscillation frequency of 300 T: here, the difference to our films may be accounted for by oxygen vacancies.

Furthermore, the SdH oscillations distinguish the epitaxial CaVO_3 films from epitaxial SrVO_3 films¹⁶, for which no quantum oscillations were reported, despite the fact that for ultraclean SrVO_3 the carrier concentration of the minority hole is large enough to cause a significant change in the Hall derivative¹⁶. Next to strain, the main difference lies in the exact perovskite structure (cubic vs. pseudo-cubic) of the two correlated metals. However, resolving this issue for SrVO_3 will require further investigations.

In the following, we discuss the non-saturating linear magnetoresistance (LMR). It is a peculiar feature of the ultraclean limit for all systems considered here^{1,2,16}. It appears strongly reduced for the disordered limit and does not occur for polycrystalline films³⁴. Classically, open orbits are the main cause of the non-saturating MR ⁴³ which has been previously proposed¹ as mechanism for CaVO_3 . In the multi-band model^{10,30} the magnetoresistance scales in general with B^2 and can have a nearly linear B -dependence only in a small magnetic-field range⁴⁴. However, the LMR is particularly observed for $\mu B > 1$. A LMR may originate from different effects. First, averaging of anisotropic mobility in polycrystalline materials^{45,46}, however, polycrystallinity can be ruled out in this study and furthermore, for polycrystalline CaVO_3 films no LMR was reported³⁴. Second, the linear *quantum* magnetoresistance⁴⁷ is rather unlikely, because it requires a majority charge carrier density of the order of 10^{18} cm^{-3} . Third, multi-band transport in combination with anisotropies, such as in SrMnBi_2 with Dirac and parabolic band states, shows non-saturating LMR⁴⁸, in which the LMR may be attributed to anisotropic scattering between the different bands. Fourth, anisotropies in k -space: orbits around sharp edges on the Fermi surface (e.g. square-like Fermi surfaces) appear as increased elastic scattering, while rounded corners produce a low-field quadratic MR dependence⁴⁵. This

is consistent for the observed LMR in the low-field regime ($\mu B < 1$) of CaVO_3 and SrVO_3 ^{16,31}, where three Fermi surfaces exist, and the outer Fermi surface is a cuboid with cylindrical openings on its side surfaces. The two inner Fermi surfaces are spherical and cubic, respectively, with the cubic surface potentially causing LMR due to its sharp edges. However, in this model the LMR does not persist for $\mu B > 1$ and saturates above $\mu B \approx 0.6$. Alternatively, impeded orbital motion⁴⁹ has been proposed to account for non-saturating LMR in the high-field regime, whereby the scattering time of the carriers undergoes a drastic change periodically. Regarding our results, this model appears to provide a possible picture consistent with multi-carrier transport in the presence of sharp edges in the three-fold Fermi surface of CaVO_3 .

In order to gain further insights, angle-dependent magnetoresistance measurement may be used to explore scattering anisotropies, and magnetic field investigations above 12 T may reveal quantum oscillations from the electron channels, and show whether the magnetoresistance saturates.

IV. CONCLUSION

In summary, we demonstrate Shubnikov-de Haas oscillations and an enhanced non-saturating linear magnetoresistance in thin coherently strained epitaxial CaVO_3 films. Our transport characterization of a series of thin films with increasing RRR (from 2 to 90) as a measure of increasing epitaxial quality, reveals that for highest film quality (ultraclean limit) electron-like carriers have a mobility of up to $6600 \text{ cm}^2 \text{ V}^{-1} \text{ s}^{-1}$ at 4.2 K, not observed for low RRR . Quantum oscillations are also intrinsic to CaVO_3 single crystals; however, they do not appear in comparable high-quality epitaxial SrVO_3 films ($RRR = 195$) prepared by the same method. This calls for detailed investigations regarding origins from the orthorhombic versus the cubic perovskite structure. A non-saturating linear magnetoresistance appears to originate from

intrinsic anisotropies and a multi-band transport, as it similarly occurs in CaVO_3 single crystals and comparable SrVO_3 thin epitaxial films. Our findings provide experimental evidence that high-quality epitaxial films of CaVO_3 , despite coherently substrate-induced small strain and increased surface scattering, display the same features as the bulk correlated metal. Transport phenomena show the delicate interplay of multiple carriers with correlations stemming from a non-spherical nested Fermi surface of a perovskite structure with orthorhombic distortion. These results thus provide fundamental insights, potentially applicable to ultra-thin film transparent electronics.

Author's contributions

M. M., M. E., O. C., and S. F. F. conceived and planned the experiments. T. K. and R. E.-H. performed the film growth. M. M. and M. E. performed the transport experiments. All authors interpreted the data. M. M., O. C., R. E.-H., and S. F. F. wrote the manuscript with the input from all authors.

Acknowledgements

M. M., M. E., R. E.-H. and S. F. F. acknowledge the support from the Leibniz-Science Campus GraFOx-II, funded by the Leibniz Association (W40/2019) and the Humboldt-Universität zu Berlin. T. K. and R. E.-H. acknowledge the support from the National Science Foundation through DMREF Grant No. DMR-1629477 for the film growth, and structural characterization. The magnetotransport data up to 12 T were taken in the Joined Lab for Advanced Magnetotransport Adlershof.

Experimental details

The CaVO_3 thin films were grown on $10 \text{ mm} \times 10 \text{ mm}$ LaAlO_3 (100) substrates ($a = 3.792 \text{ \AA}$) in a DCA M600 hybrid molecular beam epitaxy system. All details about growth and structure can be found in Ref. 21. The calcium flux of $2.5 \cdot 10^{13} \text{ atoms cm}^{-2} \text{ s}^{-1}$ was supplied via a solid-state effusion cell, while the metalorganic precursor vanadium oxitriisopropoxide (VTIP) was employed as vanadium source. Thin CaVO_3 films were grown by co-supplying Ca and VTIP using a range of different VTIP supply fluxes, quantified as VTIP gas inlet pressure P_{VTIP} . Film thickness of $38 \pm 2 \text{ nm}$ and out-of-plane lattice parameter were extracted from the high resolution XRD scans²¹. Reciprocal space maps obtained from X-ray diffraction indicate that the films are coherently strained on the substrate, exhibiting a tensile strain²¹ of 0.47 %. For electrical characterization the films were diced into $5 \text{ mm} \times 5 \text{ mm}$ and $1.25 \text{ mm} \times 5 \text{ mm}$ pieces, the first of which was used for electrical measurements in Van der Pauw geometry and the second for measurements in Hall geometry. Wire wedge-bonding was used for ohmic contacts to the films with an Al/Si (99%/1%) wire. For the measurements a Keithley 6221/2182A Complete Delta Mode system was used, combined with a Keithley 7001 switch matrix. The resistivity and Hall measurements in Van der Pauw geometry were performed in a KONTI IT Cryostat with a magnetic field of up to 700 mT. The Hall measurements were extended to 6 T using a Quantum Design Physical Property Measurement System (PPMS), with the Model 7100 AC Transport Controller for transport measurements in 5-wire Hall measurement configuration²². For the evaluation of the magnetoresistance data the antisymmetric part of the Hall resistance has been subtracted. In both cryogenic systems the ambient conditions were helium atmosphere at standard pressure. For the 12 T measurements an Oxford Instruments TeslatronPT system was used with a KelvinoxJT insert. The measurements were performed in Van der Pauw geometry and the films were kept in vacuum.

For resistivity and Hall analysis the resistance R was measured by ramping a current I from zero to its positive maximum, then to its negative maximum and back to zero. Meanwhile, the voltage was measured and the resistance was determined from the slope $R = \frac{\partial U}{\partial I}$. A sweep consisted of at least 100 points and the uncertainty for the slope of the linear model gives the uncertainty for the resistance. With this method, the uncertainty for all resistance measurements is below 0.1 %.

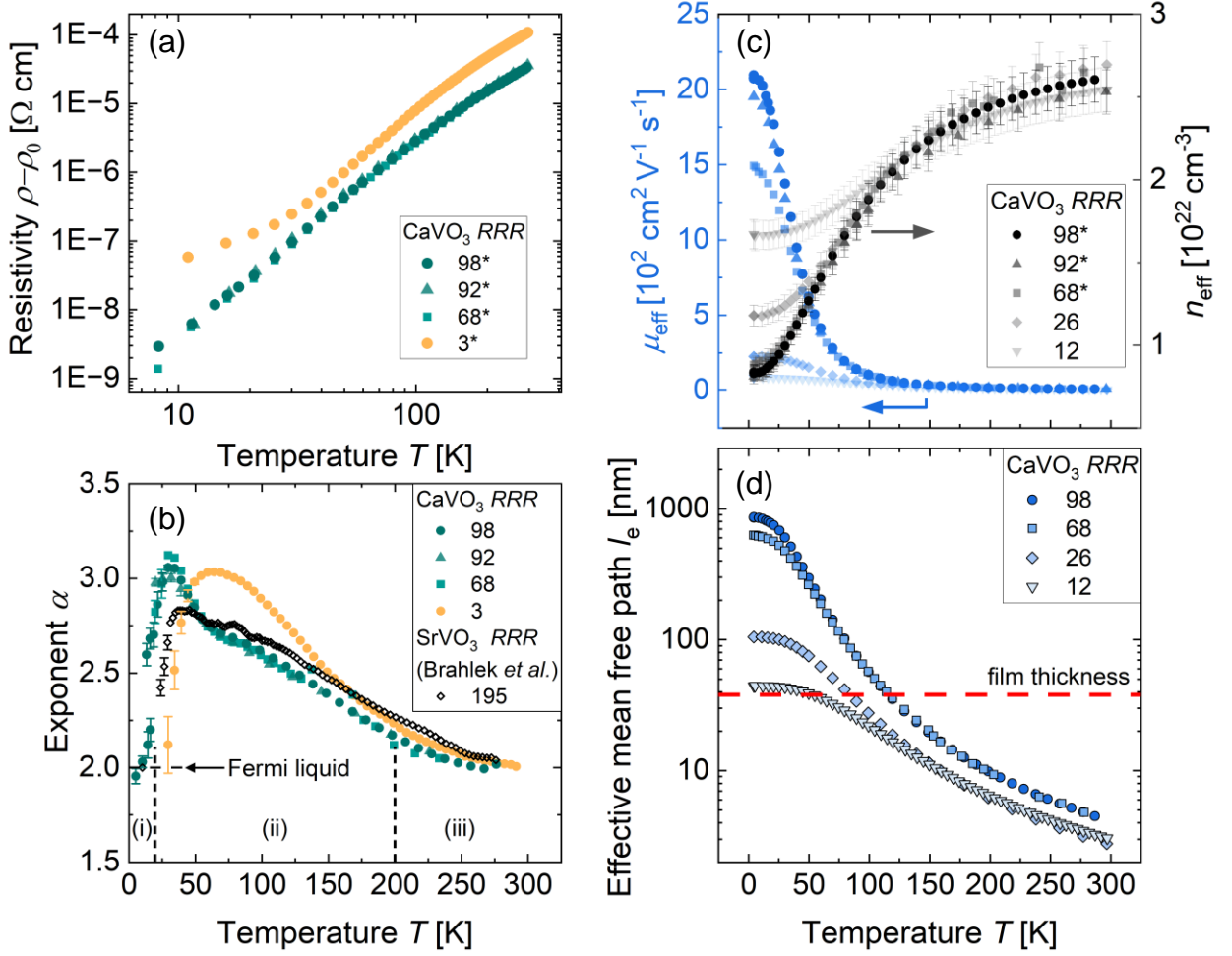


Figure 1 (a) Temperature dependent resistivity $\rho(T)$ for films with different RRR . ρ_0 is the residual resistivity. Data marked with (*) were previously published in Ref. 21. (b) Exponent α extracted from the resistivity fit $\rho(T) = \rho_0 + A \cdot T^\alpha$ for four different CaVO_3 films, and an ultraclean SrVO_3 film taken from Ref. 16. (c) Low-field inverse Hall coefficient $n_{\text{eff}} = (-eR_H)^{-1}$ and effective mobility μ_{eff} evaluated within the one-band model. For higher RRR values, the decrease of the inverse Hall coefficient and the increase in effective mobility is largest. (d) Calculated *effective* mean free path l_e (Drude picture). For films with highest RRR , l_e significantly exceeds the film thickness d (red dashed horizontal line).

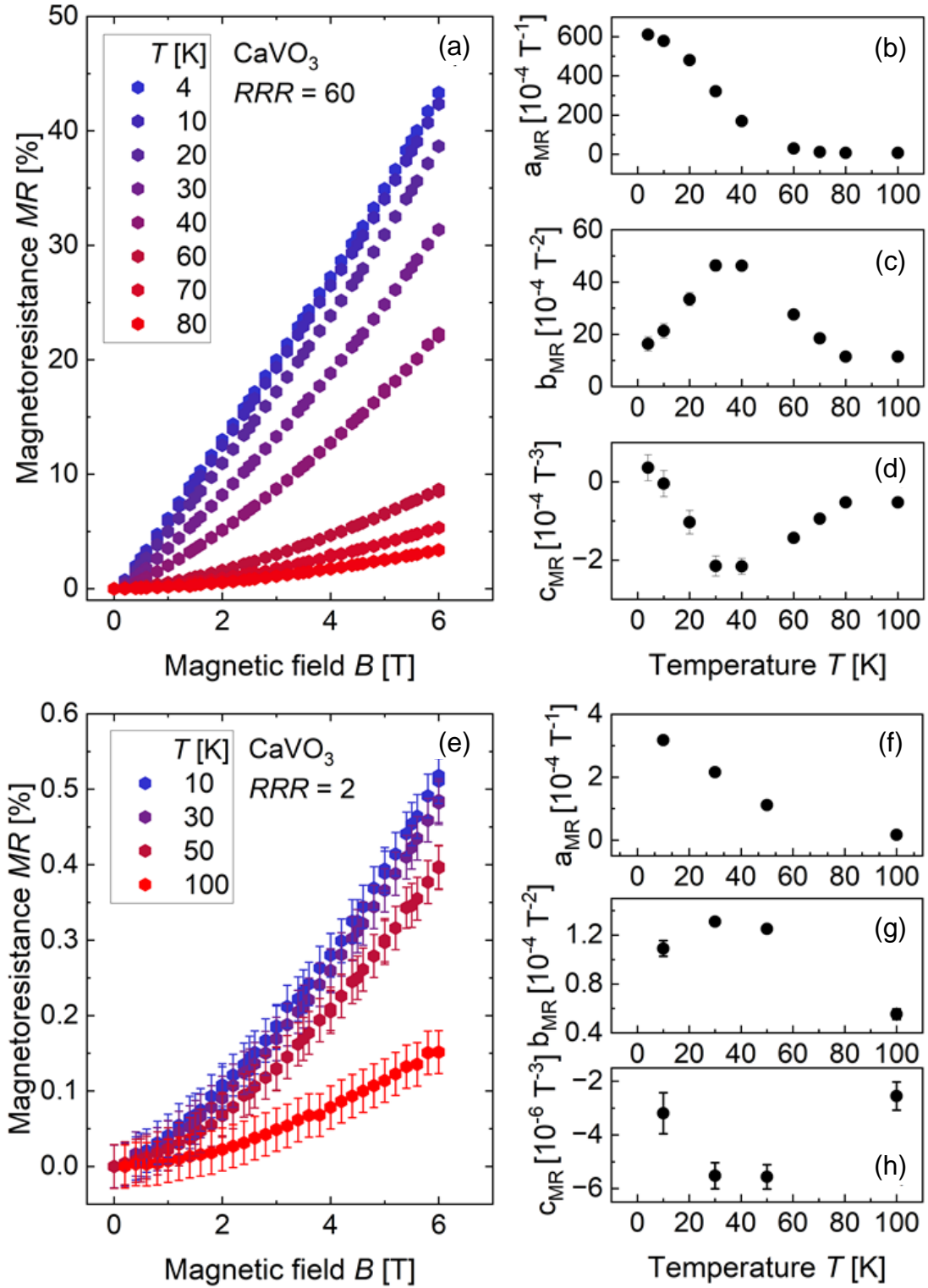


Figure 2 Magnetoresistance of CaVO₃ epitaxial thin films with (a) $RRR = 60$ and (e) $RRR = 2$ for different temperatures. The corresponding fit parameters for $MR = a_{MR}|B| + b_{MR} \cdot B^2 + c_{MR} \cdot |B^3|$ are shown in (b)-(d) and (f)-(h), respectively.

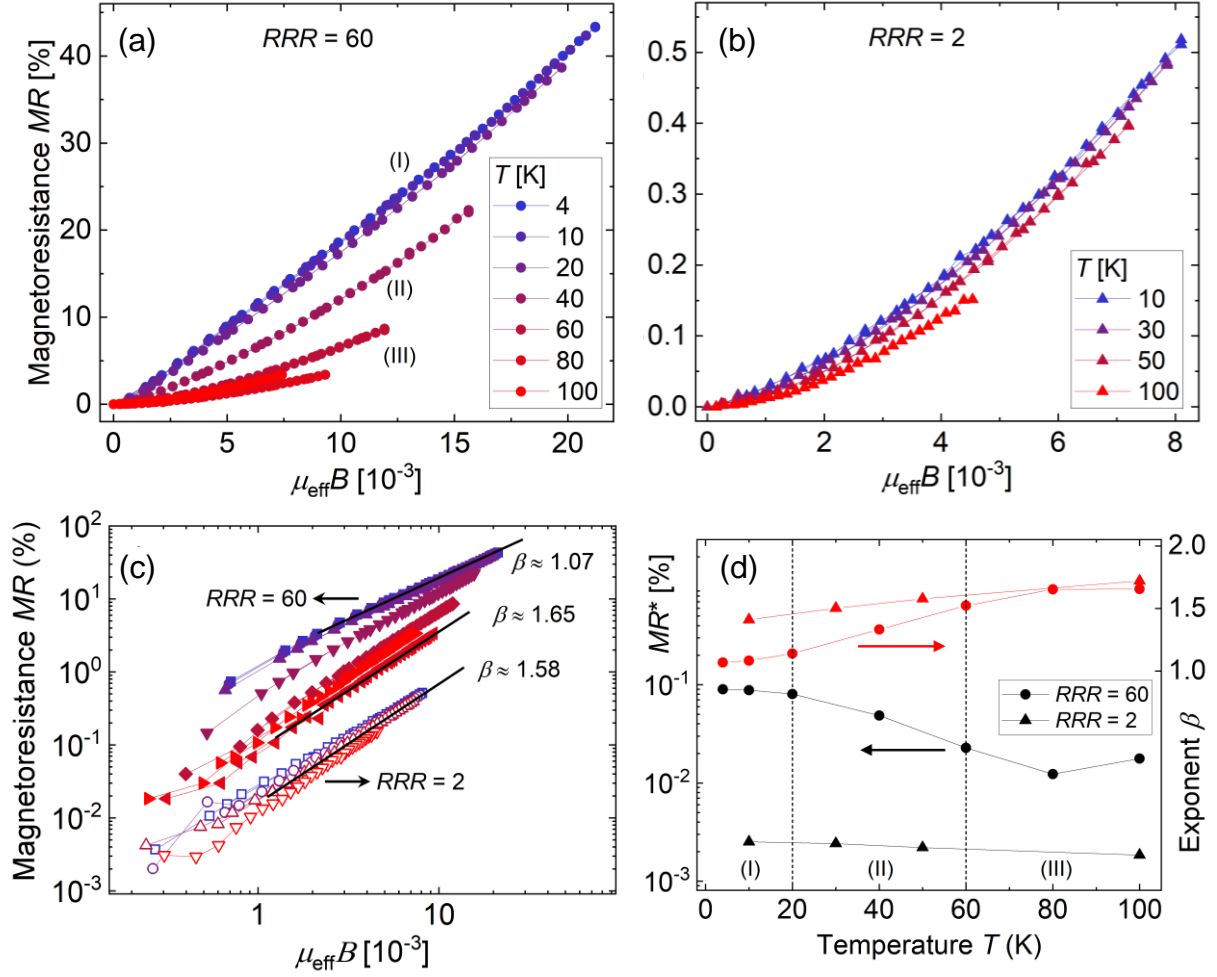


Figure 3 Magnetoresistance as a function of normalized magnetic field $\mu_{\text{eff}}B$ for CaVO₃ epitaxial thin films with (a) $RRR = 60$ and (b) $RRR = 2$, for different temperatures. (c) Data from (a) and (b) in a log-log plot to emphasize the power-law dependence on the magnetic field: $MR \propto B^\beta$. The solid lines are guides to the eye for the corresponding exponent. (d) Magnetoresistance MR^* at $\mu_{\text{eff}}B \approx 5 \cdot 10^{-3}$ and exponent β as a function of temperature.

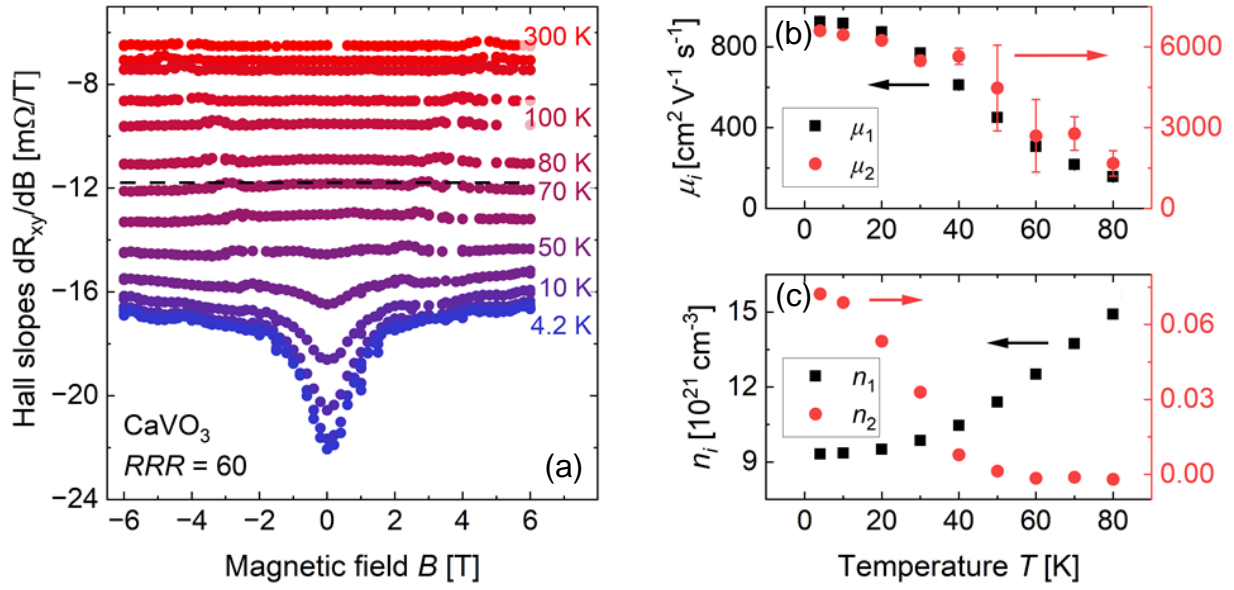


Figure 4 CaVO_3 epitaxial thin films: (a) Derivative of the Hall resistance $\frac{\partial R_{xy}}{\partial B}$ as a function of magnetic field for $RRR = 60$. (b) and (c) Results of the two-band fits of the data in (a) for the temperature-dependent mobility and carrier concentration, respectively, of two electron channels.

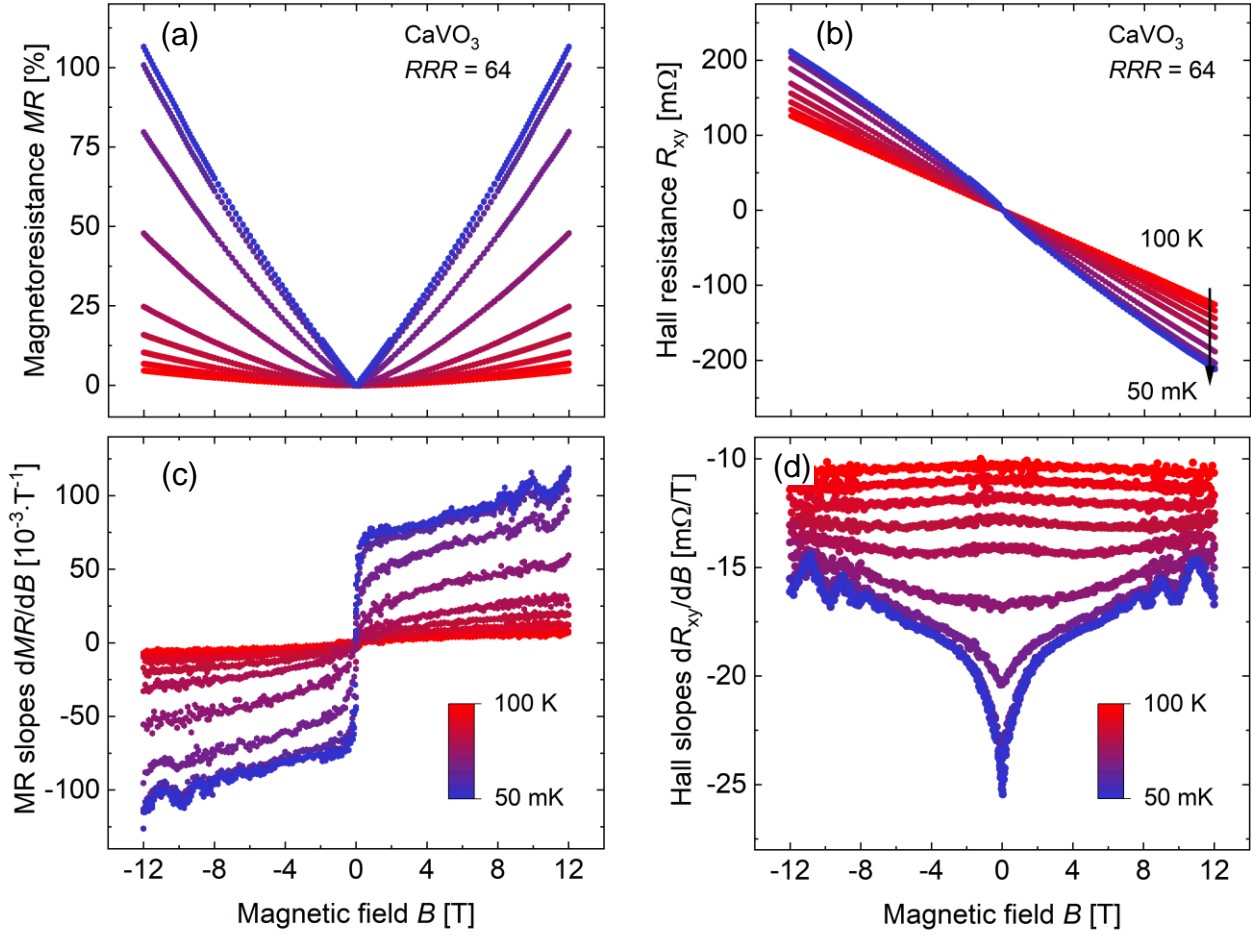


Figure 5 (a) The magnetoresistance for a CaVO_3 epitaxial thin film and (c) the mean derivative of the magnetoresistance in magnetic fields up to 12 T. (b) Hall resistances at different temperatures for a CaVO_3 epitaxial thin film and (d) the mean derivative for every temperature in magnetic fields up to 12 T. The temperatures are 100, 90, 80, 70, 60, 45, 30, 15, 0.8 and 0.05 K, respectively.

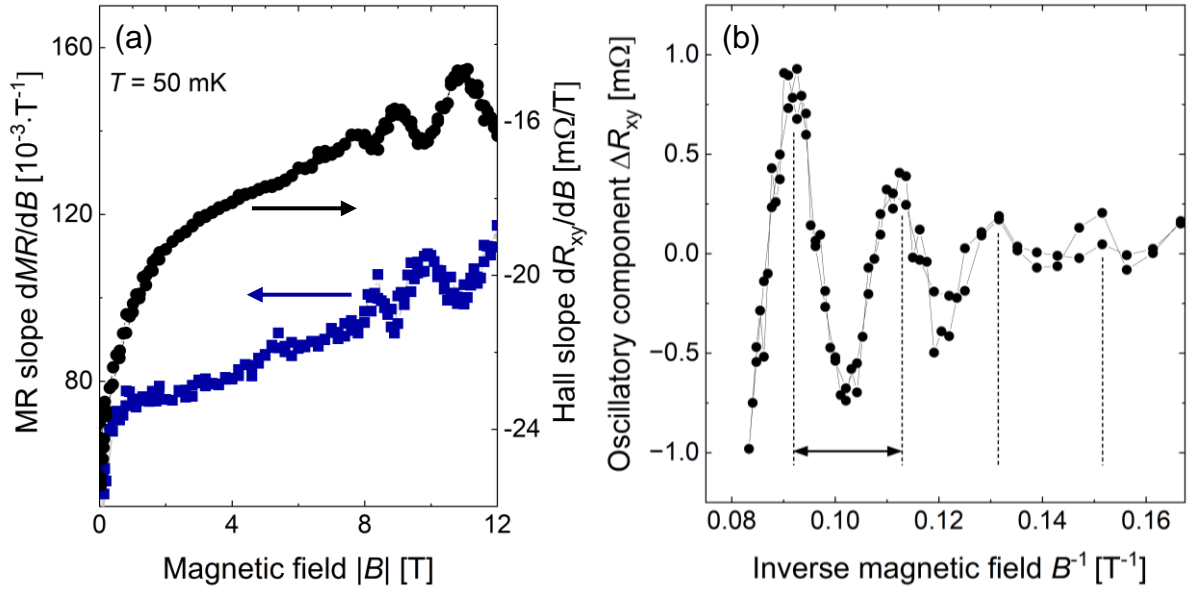


Figure 6 CaVO₃ epitaxial thin film with $RRR = 64$: (a) Magnetoresistance and Hall slope as a function of the absolute value of the magnetic field at $T = 50$ mK, showing oscillations for $B > 7$ T. (b) Oscillatory component of the Hall resistance as a function of inverse magnetic field B^{-1} at $T = 50$ mK. The Shubnikov-de Haas period is estimated to be $\Delta\left(\frac{1}{B}\right) = 0,019$ T, corresponding to a frequency of $B_{\text{sdH}} \approx 52$ T.

- ¹ M.H. Jung, I.H. Inoue, H. Nakotte, and A.H. Lacerda, “High-field properties of single-crystal CaVO_3 ,” *Philosophical Magazine B* **82**(7), 801 (2002).
- ² A. Fukushima, K. Murata, K. Morikawa, F. Iga, G. Kido, and Y. Nishihara, “Shubnikov-de Haas effect in CaVO_{3-y} ,” *Physica B Condens Matter* **194–196**(PART 1), 1161–1162 (1994).
- ³ I.H. Inoue, O. Goto, H. Makino, N.E. Hussey, and M. Ishikawa, “Bandwidth control in a perovskite-type $3d^1$ -correlated metal $\text{Ca}_{1-x}\text{Sr}_x\text{VO}_3$. 1. Evolution of the electronic properties and effective mass,” *Phys Rev B* **58**(8), 4372 (1998).
- ⁴ B.G. Lewis, and D.C. Paine, “Applications and processing of transparent conducting oxides,” *MRS Bull* **25**(8), 22 (2000).
- ⁵ G. Haacke, “Transparent Conducting Coatings,” *Annual Review of Materials Science* **7**, 73 (1977).
- ⁶ G.J. Exarhos, and X.D. Zhou, “Discovery-based design of transparent conducting oxide films,” *Thin Solid Films* **515**(18), 7025 (2007).
- ⁷ K. Ellmer, “Past achievements and future challenges in the development of optically transparent electrodes,” *Nat Photonics* **6**(12), 809–817 (2012).
- ⁸ J. Guo, C.M. Huard, Y. Yang, Y.J. Shin, K.T. Lee, and L.J. Guo, “ITO-Free, Compact, Color Liquid Crystal Devices Using Integrated Structural Color Filters and Graphene Electrodes,” *Adv Opt Mater* **2**(5), 435–441 (2014).
- ⁹ L. Zhang, Y. Zhou, L. Guo, W. Zhao, A. Barnes, H.T. Zhang, C. Eaton, Y. Zheng, M. Brahlek, H.F. Haneef, N.J. Podraza, M.H.W. Chan, V. Gopalan, K.M. Rabe, and R. Engel-Herbert, “Correlated metals as transparent conductors,” *Nat Mater* **15**(2), 204 (2016).
- ¹⁰ N. W. Ashcroft, and N. D. Mermin, *Solid State Physics* (Harcourt Brace, 1976).
- ¹¹ D. E. McNally, X. Lu, J. Pelliciari, S. Beck, M. Dantz, M. Naamneh, T. Shang, M. Medarde, C.W. Schneider, V.N. Strocov, E. V. Pomjakushina, C. Ederer, M. Radovic, and T. Schmitt, “Electronic localization in CaVO_3 films via bandwidth control,” *NPJ Quantum Mater* **4**(1), 1 (2019).
- ¹² E. Pavarini, S. Biermann, A. Poteryaev, A.I. Lichtenstein, A. Georges, and O.K. Andersen, “Mott Transition and Suppression of Orbital Fluctuations in Orthorhombic $3d^1$ Perovskites,” *The American Physical Society* **92**, 176403 (2004).
- ¹³ T. Yoshida, M. Hashimoto, T. Takizawa, A. Fujimori, M. Kubota, K. Ono, and H. Eisaki, “Mass renormalization in the bandwidth-controlled Mott-Hubbard systems SrVO_3 and CaVO_3 studied by angle-resolved photoemission spectroscopy,” *Phys Rev B Condens Matter Mater Phys* **82**(8), 085119 (2010).
- ¹⁴ A. Georges, G. Kotliar, W. Krauth, and M.J. Rozenberg, “Dynamical mean-field theory of strongly correlated fermion systems and the limit of infinite dimensions,” *Rev Mod Phys* **68**(1), 13 (1996).
- ¹⁵ M. Brahlek, A. Sen Gupta, J. Lapano, J. Roth, H.-T. Zhang, L. Zhang, R. Haislmaier, and R. Engel-Herbert, “Frontiers in the Growth of Complex Oxide Thin Films: Past, Present, and Future of Hybrid MBE,” *Adv Funct Mater* **28**(9), 1702772 (2018).
- ¹⁶ M. Brahlek, J.D. Roth, L. Zhang, M. Briggeman, P. Irvin, J. Lapano, J. Levy, T. Birol, and R. Engel-Herbert, “Hidden transport phenomena in an ultraclean correlated metal,” *Nat Commun* **15**(5304), (2024).

- ¹⁷ B.L. Chamberland, and P.S. Danielson, “Alkaline-earth vanadium (IV) oxides having the AVO_3 composition,” *J Solid State Chem* **3**(2), 243 (1971).
- ¹⁸ T. Yoshida, M. Kobayashi, K. Yoshimatsu, H. Kumigashira, and A. Fujimori, “Correlated electronic states of $SrVO_3$ revealed by angle-resolved photoemission spectroscopy,” *J. Electron Spectroscopy and Related Phenomena* **208**, 11 (2016).
- ¹⁹ I.A. Nekrasov, G. Keller, D.E. Kondakov, A. V. Kozhevnikov, T. Pruschke, K. Held, D. Vollhardt, and V.I. Anisimov, “Comparative study of correlation effects in $CaVO_3$ and $SrVO_3$,” *Phys Rev B* **72**(15), 155106 (2005).
- ²⁰ K. Maiti, D.D. Sarma, M.J. Rozenberg, I.H. Inoue, H. Makino, O. Goto, M. Pedio, and R. Cimino, “Electronic structure of $Ca_{1-x}Sr_xVO_3$: A tale of two energy scales,” *Europhys Lett* **55**(2), 246 (2001).
- ²¹ T. Kuznetsova, M. Müller, S.F. Fischer, and R. Engel-Herbert, “Toward ultraclean correlated metal $CaVO_3$,” *APL Mater* **11**(4), 041120 (2023).
- ²² Quantum Design, “AC Transport Option User’s Manual,” Part Number 1584-100, D4, (2009).
- ²³ I.H. Inoue, K. Morikawa, H. Fukuchi, T. Tsujii, F. Iga, and Y. Nishihara, “Metal-insulator transition in nearly stoichiometric $CaVO_3$,” *Jpn J Appl Phys* **32**(32–3), 451 (1993).
- ²⁴ M. Liberati, R. V. Chopdekar, V. Mehta, E. Arenholz, and Y. Suzuki, “Epitaxial growth and characterization of $CaVO_3$ thin films,” *J Magn Magn Mater* **321**(18), 2852 (2009).
- ²⁵ N. Shirakawa, K. Murata, F. Iga, Y. Nishihara, and H. Makino, “Scaling of Negative Magnetoresistance and Extraordinary Hall Effect in $CaVO_{3-\delta}$,” *J Physical Soc Japan* **64**(12), 4824 (1995).
- ²⁶ M. Gu, J. Laverock, B. Chen, K.E. Smith, S.A. Wolf, and J. Lu, “Metal-insulator transition induced in $CaVO_3$ thin films,” *J Appl Phys* **113**(133704), 1 (2013).
- ²⁷ I.H. Inoue, C. Bergemann, I. Hase, and S.R. Julian, “Fermi Surface of $3d^1$ Perovskite $CaVO_3$ near the Mott Transition,” *Phys Rev Lett* **88**(23), 236403 (2002).
- ²⁸ C. Eaton, J. Lapano, L. Zhang, M. Brahlek, and R. Engel-Herbert, “Self-regulated growth of $CaVO_3$ by hybrid molecular beam epitaxy,” *Journal of Vacuum Science & Technology A: Vacuum, Surfaces, and Films* **35**(6), 1 (2017).
- ²⁹ D. Kojda, R. Mitdank, M. Handweg, A. Mogilatenko, M. Albrecht, Z. Wang, J. Ruhhammer, M. Kroener, P. Woias, and S.F. Fischer, “Temperature-dependent thermoelectric properties of individual silver nanowires,” *Phys Rev B* **91**(2), 024302 (2015).
- ³⁰ R. Gross, and A. Marx, *Festkörperphysik* (Oldenbourg Wissenschaftsverlag Verlag, 2012).
- ³¹ M.M. Rahaman, K.M. Hossain, M.H.K. Rubel, A.K.M.A. Islam, and S. Kojima, “Alkaline-Earth Metal Effects on Physical Properties of Ferromagnetic AVO_3 (A = Ba, Sr, Ca, and Mg): Density Functional Theory Insights,” *ACS Omega* **7**(24), 20914 (2022).
- ³² Y. Obata, Y. Kohama, S. Matsuishi, and H. Hosono, “Shubnikov-de Haas oscillations in the three-dimensional Dirac fermion system Ca_3PbO ,” *Phys Rev B* **99**, 115133 (2019).
- ³³ W. G. Baber, “The contribution to the electrical resistance of metals from collisions between electrons,” *Proc A* **158**(894), 383 (1937).

- ³⁴ M. Mirjoleit, F. Rivadulla, P. Marsik, V. Borisov, R. Valentí, and J. Fontcuberta, “Electron–Phonon Coupling and Electron–Phonon Scattering in SrVO₃,” *Advanced Science* **2004207**, 1 (2021).
- ³⁵ F. Bloch, “Zum elektrischen Widerstandsgesetz bei tiefen Temperaturen,” *Zeitschrift Für Physik* **59**(3–4), 208 (1930).
- ³⁶ Z.B. Huang, W. Hanke, E. Arrigoni, and D.J. Scalapino, “Electron-phonon vertex in the two-dimensional one-band Hubbard model,” *Phys Rev B* **68**(22), 220507 (2003).
- ³⁷ M.L. Kulić, and R. Zeyher, “Influence of strong electron correlations on the electron-phonon coupling in high- T_c oxides,” *Phys Rev B* **49**(6), 4395–4398 (1994).
- ³⁸ D.J. Abramovitch, J. Mravlje, J.-J. Zhou, A. Georges, and M. Bernardi, “Respective Roles of Electron-Phonon and Electron-Electron Interactions in the Transport and Quasiparticle Properties of SrVO₃,” *Phys Rev Lett* **133**(18), 186501 (2024).
- ³⁹ C.A. Kukkonen, “Resistivity due to electron-phonon scattering on a small cylindrical Fermi surface: Application to bismuth,” *Phys Rev B* **18**(4), 1849 (1978).
- ⁴⁰ A.H. Wilson, “The electrical conductivity of the transition metals.,” *Proc R Soc Lond A Math Phys Sci* **167**(931), 580 (1938).
- ⁴¹ P.D. Desai, H.M. James, and C.Y. Ho, “Electrical Resistivity of Vanadium and Zirconium,” *J Phys Chem Ref Data* **13**(4), 1097 (1984).
- ⁴² G.K. White, and S.B. Woods, “Electrical and thermal resistivity of the transition elements at low temperatures,” *Philosophical Transactions of the Royal Society of London. Series A, Mathematical and Physical Sciences* **251**(995), 273 (1959).
- ⁴³ J.M. Ziman, *Principles of the Theory of Solids* (Cambridge University Press, 1972).
- ⁴⁴ J.S. Kim, “A matrix formalism for the Hall effect in multicarrier semiconductor systems,” *J Appl Phys* **86**(6), 3187 (1999).
- ⁴⁵ A.B. Pippard, *Magnetoresistance in Metals* (Cambridge University Press, 1989).
- ⁴⁶ M.M. Parish, and P.B. Littlewood, “Non-saturating magnetoresistance in heavily disordered semiconductors,” *Nature* **2003 426:6963 426**(6963), 162 (2003).
- ⁴⁷ A.A. Abrikosov, “Quantum linear magnetoresistance,” *Europhys. Lett* **49**(6), 789 (2000).
- ⁴⁸ X. Yan, C. Zhang, S.S. Liu, Y.W. Liu, D.W. Zhang, F.X. Xiu, and P. Zhou, “Two-carrier transport in SrMnBi₂ thin films,” *Front Phys (Beijing)* **12**(3), 1 (2017).
- ⁴⁹ R.D.H. Hinlopen, F.A. Hinlopen, J. Ayres, and N.E. Hussey, “B² to B-linear magnetoresistance due to impeded orbital motion,” *Phys Rev Res* **4**(033195), 1 (2022).